Nanomaterials

Deutsche Ausgabe: DOI: 10.1002/ange.201509752
Internationale Ausgabe: DOI: 10.1002/anie.201509752

Use of Three-Dimensional Arterial Models To Predict the In Vivo Behavior of Nanoparticles for Drug Delivery

Paninee Chetprayoon, Michiya Matsusaki, Utako Yokoyama, Takanori Tejima, Yoshihiro Ishikawa, and Mitsuru Akashi**

Abstract: *Nanomaterials have been widely used for applications in biomedical fields and could become indispensable in the near future. However, since it is difficult to optimize in vivo biological behavior in a 3D environment by using a single cell in vitro, there have been many failures in animal models. In vitro prediction systems using 3D human-tissue models reflecting the 3D location of cell types may be useful to better understand the biological characteristics of nanomaterials for optimization of their function. Herein we demonstrate the potential ability of 3D engineered human-arterial models for in vitro prediction of the in vivo behavior of nanoparticles for drug delivery. These models enabled optimization of the composition and size of the nanoparticles for targeting and treatment efficacy for atherosclerosis. In vivo experiments with atherosclerotic mice suggested excellent biological characteristics and potential treatment effects of the nanoparticles optimized in vitro.*

The estimated cost of research and development for a single new drug compound has been reported to exceed $1.8 billion,[1] and improvements in research and development productivity to reduce costs is a key challenge. One potential solution is the acceleration of the preclinical development and assessment processes. Although preclinical animal experiments are essential to test pharmacological and pharmacokinetic responses, they are usually complex, less repeatable, time consuming, and produce different results than shown in humans. These issues have also affected the development of nanomaterials. Recently, nanomaterials have been more widely applied in biomedical applications, and they could become indispensable for use in medical and diagnostic tools in the near future. However, since it is generally difficult to optimize their in vivo three-dimensional biological and physicochemical behavior by using in vitro cell assays, there have been many failures with animal models. Accordingly, if the in vivo biological properties and behavior of drugs and nanomaterials (e.g. diffusion, accumulation, and toxicity inside the target tissues) can be predicted partly in an initial in vitro assessment during drug discovery, the research and development process will be improved dramatically.

To this end, we focused on 3D tissues reconstructed in vitro and consisting of multiple cell types. Three-dimensional spheroids and other engineered tissues have been studied during toxicity and activity assays of prodrugs during drug discovery, especially for hepatic tissues.[2,3] However, engineered tissues might also be promising for the in vitro prediction of the in vivo 3D behavior of drugs and drug carriers, since 3D engineered tissues can partly replicate the 3D properties and environment of in vivo living tissues. Although physicochemical properties are usually evaluated by in vitro analysis, biological properties and 3D behavior inside tissue cannot be evaluated without in vivo animal experiments.

Herein we demonstrate the in vitro prediction of the in vivo behavior of drug-delivery nanocarriers. We have previously demonstrated the 3D diffusion of nitric oxide (NO) molecules inside 3D arterial-wall models (3D-AWMs) in response to a hormone peptide. The 3D-AWMs were composed of endothelial-cell (EC) layers and underlying multilayered smooth muscle cells (SMCs).[4] This result encouraged us to apply 3D-AWMs to the in vitro prediction of the biological properties of nanoparticles (NPs) for drug delivery. In this study, atherosclerosis and paclitaxel (PTX) were selected as a target disease and drug, respectively. Atherosclerosis, which affects the vasculature systemically, poses a serious risk to the coronary artery because rupture may lead to myocardial infarction.[5] Migration and overgrowth of SMCs occurs as a cascade of events and results in a buildup of plaques, which thicken the arterial wall.[6] Three-dimensional structures consisting of multilayered SMCs and ECs are suitable for reproducing the coronary arterial environment. Generally, monolayer cultures of vascular ECs, or coculture models of vascular ECs and SMCs, which are cultured on both sides of the substrate membrane, are used as in vitro models to study the response of cells to drugs or NPs.[7,8] For effective treatment, the drug carriers not only need to target the diseased tissue, but also to penetrate the tissue and remain long enough before being removed from the body through the blood clearance system.[9,10] We describe the in vitro prediction of the 3D penetration, accumulation, cytotoxicity, and treatment effect of NPs with 3D-AWMs and

[*] P. Chetprayoon, Dr. M. Matsusaki, Prof. M. Akashi
Department of Applied Chemistry
Graduate School of Engineering, Osaka University
Yamadaoka, Suita, Osaka 565–0871 (Japan)
E-mail: akashi@chem.eng.osaka-u.ac.jp
Homepage: http://www.chem.eng.osaka-u.ac.jp/~akashi-lab/index.html
Prof. U. Yokoyama, T. Tejima, Prof. Y. Ishikawa
Cardiovascular Research Institute
Yokohama City University, Graduate School of Medicine
3-9 Fukuura, Kanazawa-ku, Yokohama, Kanagawa 236-0004 (Japan)
E-mail: yishikaw@yokohama-cu.ac.jp

Supporting information for this article, including methods for the construction of 5L-AWMs, the synthesis of γ-PGA-NPs, permeability experiments, in vivo fluorescence imaging of NPs, and in vivo treatment experiments with a mouse model of atherosclerosis, can be found under http://dx.doi.org/10.1002/anie.201509752.

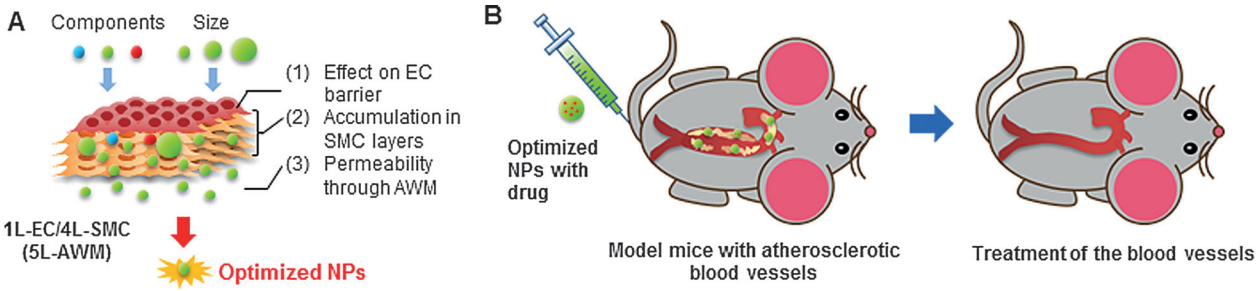

Figure 1. Overview of this study. A) Evaluation of the transport of NPs with various characteristics across the 5L-AWM (1L-EC/4L-SMC) in vitro, and the effect of the NPs on the EC barrier. B) NPs with properties optimized for their use as drug carriers were loaded with PTX and evaluated in vivo with a mouse model of atherosclerosis.

the results of a proof of concept (POC) with a mouse model of atherosclerosis (Figure 1).

3D-AWMs consisting of 1L-ECs grown on 4L-SMCs (5L-AWMs; *x*L is the number of layers) were used in this study. We previously reported PTX-loaded L-phenylalanine ethyl ester grafted poly(γ-glutamic acid) NPs (γ-PGA-NPs-PTX) with a diameter of 180 nm and evaluated their antiproliferative effect on a SMC monolayer.[11] The NPs were able to lower cell proliferation for at least 6 days in culture after incubation for only 1 h. Nevertheless, the effect of the drug in the cell monolayer was different from that in the 3D culture, and is even more distinct in vivo.[12] Accordingly, it is necessary to evaluate the effect of the NPs in 3D-AWMs to obtain more accurate results for the treatment of atherosclerosis.

SMCs are known to become a proliferative phenotype when cultured in vitro in the presence of serum protein.[8] We therefore used 5L-AWMs as a model of early-stage atherosclerosis owing to their growth during culture (see Figures S1 and S2 in the Supporting Information). The growth of 5L-AWMs during these 2 weeks was effectively suppressed when the NPs were applied for 24 h on day 1. A dose-dependent effect of the NPs on growth suppression was observed when the concentration of PTX was lower than 50 $\mu g\,mL^{-1}$. On the other hand, free PTX did not suppress growth more than γ-PGA-NPs-PTX. A single application of the NPs for 24 h was able to effectively suppress the growth of the 5L-AWMs, for at least 2 weeks, thus suggesting the accumulation of sufficient amounts of the NPs in the tissue even after washing. However, most of the free PTX was removed during washing, therefore resulting in a lower suppressive effect. In our previous study, the NPs still remained in the SMCs after incubation for 1 h and culturing for 6 days, thus suggesting rapid cellular uptake and long-term intracellular stability.[11] PTX was spontaneously released by desorption from the NPs in the physiological environment, thus suppressing cell growth. PTX is known to have high cytotoxicity to SMCs in a monolayer culture even at a concentration of 10 $ng\,mL^{-1}$.[13] In this study, the 5L-AWMs were incubated with free PTX at a concentration of 100 $\mu g\,mL^{-1}$, the concentration showing the highest suppressive effect (data not shown). However, the surviving cells proliferated, which led to thicker 5L-AWMs over the 2 weeks of culture. This result demonstrated tolerance to the drug in 3D culture. The 3D-AWMs should give more accurate results on the dose-dependent effect of the drug for the treatment of atherosclerosis.

Histological sections of the 3D-AWMs stained with anti-CD31 antibody showed the ECs inside the SMC layers after 2 weeks (see Figure S1), owing to the overgrowth of SMCs as occurs in atherosclerosis. The stable presence of ECs on the top surface was only found in the 5L-AWMs treated with NPs. We also applied the NPs to examine the treatment effect on the overgrown 4L-SMCs. The 4L-SMCs had been cultured for 5 days before the application of the NPs to enable overgrowth of the SMCs as occurs in atherosclerosis (see Figure S3). When γ-PGA-NPs-PTX (5 $\mu g\,mL^{-1}$) was applied, the growth of the structure was effectively suppressed, and the situation at day 19 seemed similar to that observed at day 11 without treatment. The therapeutic effect of the drug carriers could be estimated in vitro by use of the 3D-AWMs.

To understand the effect of the properties of the substance on cytocompatibility, we evaluated the permeability of the NPs and the barrier functions of the EC layers after applying various NPs with a similar size of approximately 50 nm, as used in our previous permeability assays (Figure 2 A,B).[14] Fluorescein-labeled γ-PGA-NPs, fluorescein isothiocyanate (FITC)-labeled polystyrene (PS) NPs, and FITC-labeled silica (Si) NPs, which are examples of biodegradable NPs, non-biodegradable NPs, and inorganic NPs, respectively, were used. All NPs exhibited a negative surface charge (the ζ potential of γ-PGA-NPs, PS-NPs, and Si-NPs was −30.6, −50.2, and −18.7 mV, respectively). Interestingly, even though all NPs were larger than the tight junctions of the EC layers (< 2 nm),[15] they showed high permeability greater than 40%. In particular, the PS-NPs exhibited the highest permeability and the lowest tendency to accumulate (see Figure S4). Kim et al. reported higher permeability of EC monolayers when treated with tumor necrosis factor-α (TNF-α), which induces the disruption of intercellular junctions (e.g. adherens junctions): the same conditions as inflammation (atherosclerosis).[16] Cellular uptake of γ-PGA-NPs and PS-NPs could be observed after incubation for 24 h. Si-NPs did not show significant cellular uptake, but became a cluster (< 30 μm in size) owing to their slight lower dispersibility in the culture medium. Damaged 5L-AWMs were found by confocal laser scanning microscopy (CLSM), which showed detachment, collapse, and reduced thickness of the AWMs after treatment with Si-NPs (Figure 2 B and see Figure S5 for

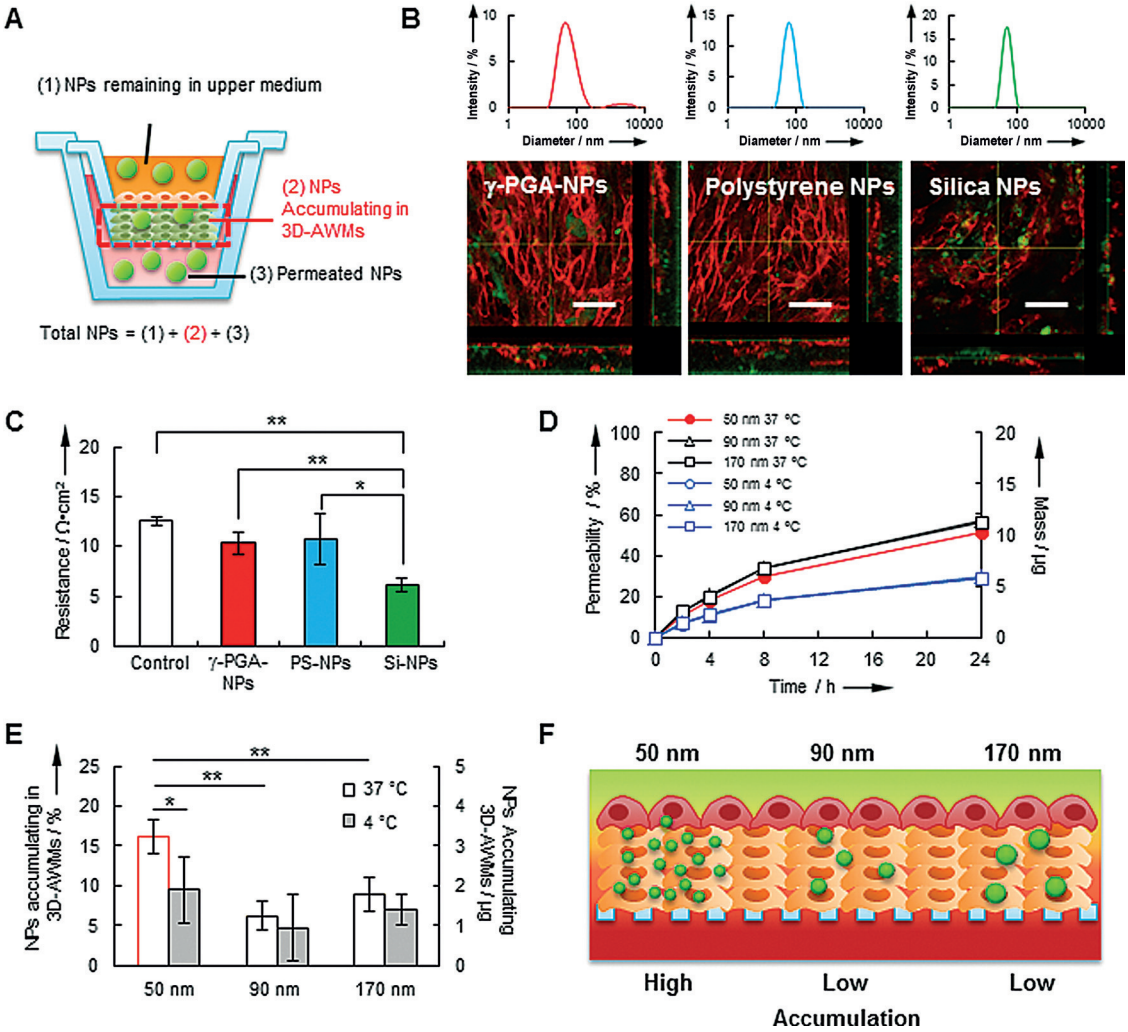

Figure 2. In vitro optimization of NPs by the use of 5L-AWMs. A) Method for evaluating the concentration of NPs accumulating in the 3D-AWMs. This concentration was determined from the concentration of NPs remaining in the upper chamber and the concentration of NPs permeated below the chamber. B) Z-stack CLSM images of 5L-AWMs after incubation for 24 h with FITC-labeled NPs. The ECs were stained with CD31 (red). Scale bars are 50 μm. Size distributions of each NP were measured by DLS. C) TEER of the 5L-AWMs after 24 h permeability experiments with each NP. The control is a 5L-AWM before the permeability test. D) Permeability of γ-PGA-NPs across the 5L-AWMs at 37 and 4 °C. E) Size effect of γ-PGA-NPs on accumulation in the 5L-AWMs after 24 h permeability experiments at 37 and 4 °C. F) Illustration showing the size effects on accumulation in the 3D-AWMs. Error bars are the standard deviation from $n=4$ (C) or $n=3$ (D and E), $^{**}p<0.01$ and $^{*}p<0.05$ denote a statistically significant difference.

larger images). The cytotoxicity of the Si-NPs might be due to the generation of reactive oxygen species (ROS), which induce cell death and could be a potential causative factor in cardiovascular diseases.[17] Although transendothelial electrical resistance (TEER) of the 5L-AWMs also significantly decreased after treatment with Si-NPs owing to damage to the tight junctions of the EC layer, γ-PGA-NPs and PS-NPs did not produce any change (Figure 2C). Because of the greater accumulation and biodegradability of γ-PGA-NPs, they were employed for further study.

γ-PGA-NPs with different sizes of 50, 90 (ca. 100), and 170 nm (ca. 200 nm) were used to study the size effect at the nanoscale on permeability and accumulation as observed in dextrans.[14] The concentration of NPs remaining in the upper chamber decreased gradually (see Figure S6), but there was no obvious size effect on permeability (Figure 2D). To investigate the mechanisms responsible for permeability, a permeability experiment was performed at 4 °C to reduce the effect of energy-dependent endocytosis.[18] As expected, higher NP concentrations were found to remain in the upper chamber (see Figure S6), and the permeability of all NPs at 4 °C was lower than that at 37 °C (Figure 2D), thus possibly suggesting endocytosis. However, since the morphology of the EC layer was also affected by this temperature, some of the NPs might have permeated across it.

Since the accumulation of NPs into atherosclerotic plaques is important for the sustainable release of PTX, the amount of NPs remaining in the 3D-AWMs was evaluated. Interestingly, at 37 °C, there were more 50 nm NPs remaining (accumulating) in the 5L-AWMs than larger NPs (Figure 2E).

A slightly lower amount of 50 nm NPs was found to permeate into the lower chamber because some of them remained inside the 5L-AWMs (Figure 2D). The smaller NPs might become more easily trapped in the nano-meshwork structures of the extracellular matrix (ECM) inside the 5L-AWMs. Experiments performed at 4 °C showed that the temperature also affected the accumulation of 50 nm NPs, thus suggesting that many of the accumulated NPs might have been taken up by the cells at 37 °C (Figure 2E,F). The remaining NPs in the 5L-AWMs were observed by CLSM even after the washing and staining processes (see Figure S7), thus indicating stable accumulation in the tissue.

To confirm this in vitro finding of the size effect on the accumulation of γ-PGA-NPs in 3D-AWMs, we investigated the in vivo accumulation of γ-PGA-NPs by using a mouse model of atherosclerosis. We examined the aorta with an in vivo imaging system (IVIS) 24 h after the injection of three different sizes of γ-PGA-NPs chemically conjugated to the dye Alexa633[19] (Figure 3A). Interestingly, as expected from the in vitro results, the strongest fluorescence intensity was found in the smallest (60 nm) NPs (the particle sizes were changed slightly by Alexa633 conjugation), with results for the highest in vivo accumulation of plaques that matched the in vitro results for the 3D-AWMs (Figure 3B). The location of

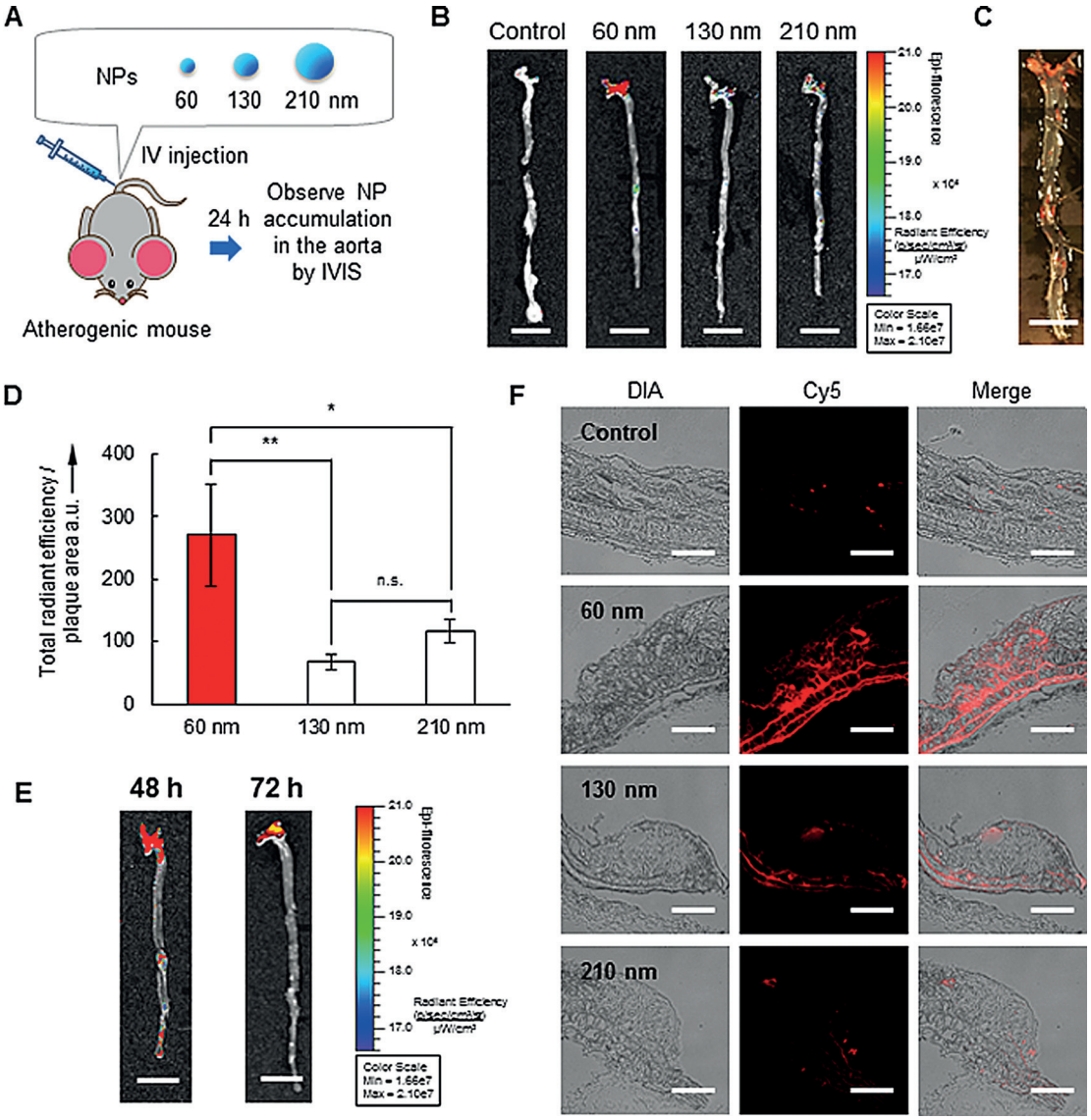

Figure 3. In vivo size effect of in vitro optimized Alexa633-conjugated γ-PGA-NPs. A) Illustration of the experimental procedure (IV = intravenous). B) IVIS images of aortas 24 h after the IV injection of each NP. The control was PBS injection (PBS = phosphate-buffered saline). C) Oil Red O stained aorta of the mouse before NP injection. D) Normalized intensity of the total radiant efficiency per plaque area for each NP size 24 h after injection ($n = 5$–7/group). $*p < 0.05$ and $**p < 0.01$ denote statistically significant differences from one-way analysis of variance according to the Newman–Keuls method; n.s. is not statistically significant. E) Accumulation of 60 nm NPs in the atherosclerotic plaques 48 and 72 h after injection. F) Frozen sections of atherosclerotic plaques 24 h after the injection of NPs. The top part of each section is the vascular lumen. Scale bars are 5 μm (B, D, and E) and 100 μm (F).

the NPs matched well with the positions of the plaques, as deduced from Oil Red O staining, thus showing lipid accumulation (Figure 3C). The intensity in the plaques was significantly higher for 60 nm NPs than for the other two larger sizes (Figure 3D). More importantly, whereas the 130 and 210 nm NPs could no longer be observed in the plaques after 48 h, the 60 nm NPs were still found to be in the plaques after 72 h, even though the intensity had become slightly weaker (Figure 3E). This result showed that 60 nm NPs have good stability in vivo, as opposed to liposomes, which accumulated in the plaques but rapidly disappeared within 8 h.[20] It has been reported that the destabilization of liposomes occurs immediately after their injection into the body owing to the fatty exchange of phospholipids in the cell membrane.[21] The 60 nm NPs were found near the plaques and medial layer, in much larger amounts as compared to the 130 and 210 nm NPs, similar to the findings by IVIS (Figure 3F). Elastica Masson trichrome (E-MT) staining of the frozen sections also indicated that the NPs were located both in lipid-rich plaque areas and in the elastic fibers (see Figure S8). As a result, the NPs remained in the plaques and were not easily removed over 72 h, thus suggesting that γ-PGA-NPs with a size of about 50 nm could be a potential drug-delivery carrier for the treatment of atherosclerosis.

Since the smallest NPs showed the highest accumulation, 60 nm NPs were used in in vivo treatment experiments. Early-stage atherogenic mice were treated weekly with γ-PGA-NPs-PTX at a PTX dose of 2.5 mg kg^{-1} for a total of 6 weeks (see Figure S9). There was no difference in the body weight of the treated and control mice; hence, the NPs-PTX did not seem to give rise to severe toxicity at the given dose. The NPs were found to have accumulated in the atherosclerotic lesions even though it had been 1 week since the final NP injection (see Figure S9), thus suggesting their long-term accumulation and stability in the plaques. Cross-sections of the plaques showed that the NPs were still located in the plaques 6 weeks after treatment (see Figure S10), which was similar to the results in Figure 3F. The treated aortae showed a reduction in the total area of the plaques. Although this difference was not statistically significant, the 60 nm γ-PGA-NPs-PTX demonstrated a potential suppressive effect on the development of atherosclerosis in vivo (see Table S1 in the Supporting Information). The treated aortae showed distinct staining that appeared denser in the presence of elastic fibers and smooth muscle layers, thus indicating less damage to the aortic wall. Images of Oil Red O stained samples showed an abundance of lipids in the plaques of the nontreated mice, whereas fewer lipids were observed in the treated mice. Furthermore, decreased thickness of the plaques was also observed in treated mice, thus suggesting that γ-PGA-NPs-PTX is an effective treatment. The results of biodistribution of the NPs showed a typical distribution, with those larger than 50 nm usually detected mostly in the liver (see Figure S11).[19,22]

In summary, we were able to predict the biological behavior of the NPs in a 3D environment by using 3D-AWMs in vitro. From our experiments with in vitro 3D-AWMs, we discovered that the size of the drug carrier plays an important role in tissue accumulation. Notably, the size effect on accumulation in the 3D-AWMs agreed with the in vivo results. We successfully conducted a POC by using 3D engineered tissues for the prediction of the in vivo 3D biological behavior of the drug carriers. Since the 3D-AWMs showed heterogeneous aggregation in response to macrophages,[23] the system has great potential as a model for mid- or late-stage atherosclerosis.

Acknowledgements

We are grateful to Ayami Hiura (Osaka University) for providing the histological sections of the 3D-AWMs. This research was mainly supported by the NEXT Program (LR026) and partially by a Grant-in-Aid for Scientific Research (S) (A232250040), the SENTAN-JST Program (13A1204), a Grant-in-Aid for Scientific Research on Innovative Areas (21106514 and 26106717), and a Grant-in-Aid for Challenging Exploratory Research.

Keywords: cell adhesion · drug delivery · layered compounds · nanoparticles · thin films

How to cite: *Angew. Chem. Int. Ed.* **2016**, *55*, 4461–4466
Angew. Chem. **2016**, *128*, 4537–4542

[1] S. M. Paul, D. S. Mytelka, C. T. Dunwiddie, C. C. Persinger, B. H. Munos, S. R. Lindborg, A. L. Schacht, *Nat. Rev. Drug Discovery* **2010**, *9*, 203–214.
[2] S. R. Khetani, S. N. Bhatia, *Nat. Biotechnol.* **2008**, *26*, 120–126.
[3] Y. Kim, P. Rajagopalan, *PLoS One* **2010**, *5*, e15456.
[4] M. Matsusaki, S. Amemori, K. Kadowaki, M. Akashi, *Angew. Chem. Int. Ed.* **2011**, *50*, 7557–7561; *Angew. Chem.* **2011**, *123*, 7699–7703.
[5] *National Heart, Lung, and Blood Institute, Fact Book Fiscal Year 2012*, National Institutes of Health, Bethesda, MD, **2012**.
[6] P. Libby, *Nature* **2002**, *420*, 868–874.
[7] T. Ziegler, R. W. Alexander, R. M. Nerem, *Ann. Biomed. Eng.* **1995**, *23*, 216–225.
[8] S. L. Rose, J. E. Babensee, *Ann. Biomed. Eng.* **2007**, *35*, 1382–1390.
[9] M. E. Lobatto, V. Fuster, Z. Fayad, W. J. M. Mulder, *Nat. Rev. Drug Discovery* **2011**, *10*, 835–852.
[10] T. T. Goodman, C. P. Ng, S. H. Pun, *Bioconjugate Chem.* **2008**, *19*, 1951–1959.
[11] P. Chetprayoon, F. Shima, M. Matsusaki, T. Akagi, M. Akashi, *Chem. Lett.* **2014**, *43*, 1767–1769.
[12] H. J. Khoury, G. Garcia-Manero, G. Borthakur, T. Kadia, M. C. Foudray, M. Arellano, A. Langston, B. Bethelmie-Bryan, S. Rush, K. Litwiler, S. Karan, H. Simmons, A. L. Marcus, M. Ptaszynski, H. Kantrjian, *Cancer* **2012**, *118*, 3556–3564.
[13] D. I. Axel, W. Kunert, C. Göggelmann, M. Oberhoff, C. Herdeg, A. Küttner, D. H. Wild, B. R. Brehm, R. Riessen, G. Köveker, K. R. Karsch, *Circulation* **1997**, *96*, 636–645.
[14] P. Chetprayoon, M. Matsusaki, M. Akashi, *Biochem. Biophys. Res. Commun.* **2014**, *456*, 392–397.
[15] J. M. Tarbell, *Cardiovasc. Res.* **2010**, *87*, 320–330.
[16] Y. Kim, M. E. Lobatto, T. Kawahara, B. L. Chung, A. J. Mieszawska, B. L. Sanchez-Gaytan, F. Fay, M. L. Senders, C. Calcagno, J. Becraft, M. T. Saung, R. E. Gordon, E. S. G. Stroes, M. Ma, O. C. Farokhzad, Z. A. Fayad, W. J. M. Mulder, R. Langer, *Proc. Natl. Acad. Sci. USA* **2014**, *111*, 1078–1083.
[17] J. Duan, Y. Yu, Y. Li, Y. Yu, X. Zhou, P. Huang, Z. Sun, *PLoS One* **2010**, *8*, e62087.

[18] K. Sandvig, S. Olsnes, *Exp. Cell Res.* **1979**, *121*, 15 – 25.
[19] R. Toita, K. Nakao, A. Mahara, T. Yamaoka, M. Akashi, *Bioorg. Med. Chem.* **2013**, *21*, 6608 – 6615.
[20] S. Chono, *Yakugaku Zasshi* **2007**, *127*, 1419 – 1430.
[21] W. W. Sułkowski, D. Pentak, K. Nowak, A. Sułkowska, *J. Mol. Struct.* **2005**, *744 – 747*, 737 – 747.
[22] W. H. De Jong, W. I. Hagens, P. Krystek, M. C. Burger, A. J. Sips, R. E. Geertsma, *Biomaterials* **2008**, *29*, 1912 – 1919.
[23] R. Ishiwata, U. Yokoyama, M. Matsusaki, Y. Asano, K. Kadowaki, Y. Ichikawa, M. Umemura, T. Fujita, S. Minamisawa, H. Shimoda, M. Akashi, Y. Ishikawa, *Atherosclerosis* **2014**, *233*, 590 – 600.

Received: October 19, 2015
Revised: February 2, 2016
Published online: March 1, 2016

